

Will New Horizons see dust clumps in the Edgeworth-Kuiper belt?

Christian Vitense
and

Alexander V. Krivov
and

Torsten Löhne

Astrophysikalisches Institut, Friedrich-Schiller-Universität Jena, Schillergäßchen 2–3, 07745 Jena, Germany
vitense@astro.uni-jena.de

ABSTRACT

Debris disks are thought to be sculptured by neighboring planets. The same is true for the Edgeworth-Kuiper debris disk, yet no direct observational evidence for signatures of giant planets in the Kuiper belt dust distribution has been found so far. Here we model the dust distribution in the outer solar system to reproduce the dust impact rates onto the dust detector onboard the New Horizons spacecraft measured so far and to predict the rates during the Neptune orbit traverse. To this end, we take a realistic distribution of transneptunian objects to launch a sufficient number of dust grains of different sizes and follow their orbits by including radiation pressure, Poynting-Robertson and stellar wind drag, as well as the perturbations of four giant planets. In a subsequent statistical analysis, we calculate number densities and lifetimes of the dust grains in order to simulate a collisional cascade. In contrast to the previous work, our model not only considers collisional elimination of particles, but also includes production of finer debris. We find that particles captured in the 3:2 resonance with Neptune build clumps that are not removed by collisions, because the depleting effect of collisions is counteracted by production of smaller fragments. Our model successfully reproduces the dust impact rates measured by New Horizons out to ≈ 23 AU and predicts an increase of the impact rate of about a factor of two or three around the Neptune orbit crossing. This result is robust with respect to the variation of the vaguely known number of dust-producing scattered disk objects, collisional outcomes, and the dust properties.

Subject headings: Kuiper belt: general, methods: numerical, methods: statistical, minor planets, asteroids: general, planet-disk interactions

1. INTRODUCTION

The symbiosis between debris disks and planets is multifaceted. Not only do both represent natural outcomes of the planetesimal and planet accretion processes, it has also long been realized that planets should sculpt the disks by their gravity, and thus the observed structure in debris disks can be used as a tracer of planets. In one case — β Pic — the observed disk structure has been undoubtedly attributed to interactions with a directly imaged planet (Lagrange et al. 2009, 2010, 2012). In a few other cases, such as Fomalhaut (Kalas et al. 2008, 2013), HR 8799 (Su et al. 2009), and HD 95086 (Rameau et al. 2013), the relation between the disks and directly imaged planets has yet to be understood. Many more systems have been found where resolved debris disks reveal various types of structure, possibly driven by gravity of unseen planets orbiting in the disks' inner cavities, exemplified by the clumpy disk of ϵ Eri (Greaves et al. 2005) or spirals in the HD 141569 disk (Wyatt 2005). However, some of these features are yet to be confirmed observationally, for instance requiring disambiguation with possible background objects. Also, models of planet-induced structure in the disk suffer from many uncertainties, especially those arising from poorly known dust properties and from difficulties of in-

cluding collisions into the models. Besides, alternative explanations of the observed disk structure that do not require the presence of planets are possible (e.g. Artymowicz & Clampin 1997; Grigorieva et al. 2007; Debes et al. 2009).

It is natural and tempting to look at our solar system. Here, the orbits and masses of planets are precisely known. Largely known are also the populations of parent bodies, maintaining its debris disk, which include asteroids, comets, and Edgeworth-Kuiper belt (EKB) objects (EKBOs). Less well known are the properties of the dust cloud that these parent bodies replenish and maintain. Yet a dust ring encompassing the Earth orbit has been discovered and its structure successfully ascribed to resonant interactions between dust grains and the Earth (Dermott et al. 1994). In the outer solar system, it has been predicted that Neptune should create two dusty clumps just exterior to its orbits, one ahead and one behind the planet slightly outside its orbit (Liou & Zook 1999). The simulated images of those clumps from the Liou & Zook (1999) paper have been used in dozens of subsequent papers as a vivid prototype of what can also be expected in extrasolar debris disks.

However, the predicted EKB clumps are still lacking direct observational confirmation. Remote observations of thermal

emission are hampered by an extremely low dust density in the EKB debris disk (Vitense et al. 2012), which causes the foreground emission of the zodiacal cloud to outshine the thermal flux from the EKB dust. Luckily, the New Horizons spacecraft is now on its way to the outer solar system. Onboard, beside several other instruments, is the Venetia Burney Student Dust Counter (SDC), capable of measuring impacts of grains between $10^{-12} \text{ g} < m < 10^{-9} \text{ g}$ in mass (Horányi et al. 2008). New Horizons will traverse the trailing clump around early 2015 and might see a dust enhancement there.

This paper addresses the question of whether the SDC has chances to detect the dust clump, proving its existence, and whether the expected data can be used to constrain the models. So far, there have been several attempts to model the EKB dust clumps (e.g., Liou & Zook 1999; Moro-Martín & Malhotra 2002, 2003; Kuchner & Stark 2010; Poppe et al. 2010; Han et al. 2011). However, most of these studies ignored possible effects of grain-grain collisions. Kuchner & Stark (2010) did include them with the aid of their novel “collisional grooming” algorithm. Nevertheless, the collisions in their model only acted to eliminate the colliders; it is not surprising therefore that the collisions in their model tends to erase the clumps. Including collisional *production* of fine debris might counteract this, putting dust enhancements back into play; we check this in this paper. Besides, none of the previous studies provided detailed predictions for the dust impact rates for the SDC detector aboard New Horizons along its trajectory; we do this here. We also try to use a more realistic “true” distribution of the EKB objects, acting as parent bodies for the dust (Vitense et al. 2010), and to include perturbations of all four giant planets.

Section 2 describes the procedure and results of the modeling in a collisionless approximation. Section 3 does the same with the collisions included. Conclusions are made in section 4 and discussed in section 5.

2. COLLISIONLESS MODEL

2.1. Method

In the spirit of previous studies (e.g., Liou & Zook 1999; Moro-Martín & Malhotra 2003; Kuchner & Stark 2010) we released dust grains from EKBOs and followed them with numerical integrations. The first step was to set the distribution of the parent bodies. Instead of using an artificial distribution, we invoked the debiased EKB distribution of Vitense et al. (2010, their Figure 5). They developed an algorithm to remove observational biases from the orbital elements of EKBOs listed in various EKBO discovery surveys. The corrected distributions of semimajor axis a , eccentricity e , and inclination i in each of three populations as defined in their paper (classical Kuiper belt, CKB; resonant objects, RES; and scattered objects, SDO) were approximated by gaussian functions. The mean values \bar{a} , \bar{e} , and \bar{i} along with the standard deviations σ_a , σ_e , and σ_i are listed in Table 1. The longitude of the ascending node, the argument of pericenter, and the mean anomaly were assumed to be uniformly distributed between 0° and 360° .

From each of the three populations we started 1000 single particles of nine different sizes, selected as described below, so that a total of 27000 particles were handled. After release, each particle feels direct solar radiation pressure, causing the initial

Table 1: Initial orbital distribution for parent bodies for classical (CKB), resonant (RES) and scattered (SDO) objects.

Population	\bar{a} [AU]	σ_a [AU]	\bar{e}	σ_e	\bar{i} [°]	σ_i [°]
CKB	43	2.5	0.0	0.1	0	17
RES	39	0.5	0.2	0.1	15	10
SDO	60	10	0.45	0.15	20	10

grain orbit to differ from that of the parent body (Burns et al. 1979). The particle orbit acquires a larger semimajor axis and typically, but not always, a larger eccentricity than those of the parent EKBO. We have included this effect with the aid of Eqs. (19)-(20) of Krivov et al. (2006).

The orbital evolution of particles was followed by numerically integrating their equations of motion with a Bulirsch-Stoer routine with an adaptive stepsize control and an accuracy parameter of 10^{-11} (Press et al. 1992). We took into account perturbations from Neptune, Uranus, Saturn, and Jupiter (the planets did not interact mutually), the Poynting-Robertson (PR) force, as well as the stellar wind drag which was assumed to have the strength of 33% of the PR effect (Gustafson 1994). The integration was stopped when the particle was ejected from the system ($r > 300 \text{ AU}$) or impacted onto a planet or the sun. The position (x, y, z) , velocity (v_x, v_y, v_z) , and time t since release of the dust grains were recorded once every orbit of Neptune, as was also done in the previous studies (Liou & Zook 1999; Moro-Martín & Malhotra 2003; Kuchner & Stark 2010). Since the dust production and loss rates are assumed to be constant, the system is ergodic. Therefore, different records of the same simulated particle can be interpreted as the same-time records of different physical grains launched at different time instants in the past. This effectively increases the number of records of our simulations to $\approx 2 \times 10^9$ for all three parent populations and nine sizes.

To set the sizes of the particles for simulations, we made use of the ratio of direct radiation pressure and gravity, β (Burns et al. 1979). The radiation pressure efficiency for the grains was calculated using the Bruggeman mixing rule and standard Mie theory (Bohren & Huffman 1983), assuming three different mixtures of astrosilicate (Laor & Draine 1993) and water ice Warren (1984). These were a 50%-50% astrosilicate-ice mixture with a bulk density of $\rho = 2.35 \text{ g cm}^{-3}$, a 10%-90% astrosilicate-ice mixture ($\rho = 1.43 \text{ g cm}^{-3}$), and pure ice ($\rho = 1.00 \text{ g cm}^{-3}$). We then selected nine equally spaced logarithmic size (or mass) bins covering the mass range which can be detected by the dust counter onboard the New Horizons spacecraft ($10^{-12} \text{ g} < m < 10^{-9} \text{ g}$, Horányi et al. 2008). The list of β values and corresponding grain sizes and masses for the three mixtures is given in Table 2.

2.2. Results

We binned the positions of particles, separately for each of the sizes, into an (x, y) -grid with $\Delta x = \Delta y = 1 \text{ AU}$. The numbers of records in each bin originating from CKB, RES, and SDO were weighted as 1 : 0.2 : 1, which is approximately the mass ratio of these populations in the “true” EKB of Vitense et al. (2010). The resulting snapshots of the dust distribution are shown in Figure 1. These are nearly identical to those published and discussed in

Table 2: β -ratios, sizes, and masses of grains used in the simulations for different material mixtures.

#	β	$\rho = 2.35 \text{ g cm}^{-3}$		$\rho = 1.43 \text{ g cm}^{-3}$		$\rho = 1.00 \text{ g cm}^{-3}$	
		$s [\mu\text{m}]$	$m [\text{g}]$	$s [\mu\text{m}]$	$m [\text{g}]$	$s [\mu\text{m}]$	$m [\text{g}]$
0	0.576	0.43	7.5E-13	0.30	1.7E-13	0.46	4.1E-13
1	0.404	0.65	2.7E-12	0.65	1.6E-12	0.69	1.4E-12
2	0.259	0.99	9.5E-12	1.05	7.0E-12	1.25	8.2E-12
3	0.164	1.51	3.4E-11	1.60	2.5E-11	1.78	2.4E-11
4	0.106	2.30	1.2E-10	2.45	8.8E-11	2.57	7.1E-11
5	0.070	3.51	4.3E-10	3.60	2.8E-10	3.45	1.7E-10
6	0.046	5.42	1.6E-9	5.80	1.2E-9	4.60	4.1E-10
7	0.029	8.59	6.2E-9	10.3	6.6E-9	6.76	1.3E-9
8	0.018	14.3	2.9E-8	18.3	3.8E-8	10.0	4.2E-9

detail previously (e.g., by Liou & Zook 1999; Kuchner & Stark 2010), and thus are summarized below only briefly.

Most of the dust is confined to a ring-like structure between slightly interior to the Neptune orbit and the outer edge of the classical EKB. This ring has an extended gap around the position of Neptune, and two broad clumps created by grains trapped in mean-motion resonances with Neptune. These resonant structures are more pronounced for larger particles since their probability to be captured into a mean-motion resonance is higher (e.g., Wyatt 2003; Mustill & Wyatt 2011). The distribution of small particles, just above the blowout limit, is more uniform. Note that not all of the $\beta = 0.576$ particles in Fig. 1 are in blowout orbits, because the parent body orbits are generally eccentric. A grain released from an eccentric orbit near the aphe- lion can stay in bound orbit even if $\beta > 0.5$.

Outside the main belt, the number density rapidly decreases, reflecting the fact that even the dust grains produced by the scattered objects are located most of their time in the main belt. Inside the main belt, the dust density also drops significantly. Noteworthy, though not sufficiently discussed in the previous papers, is the fact that the clumps of the 3 : 2 resonance have relatively sharp inner edges slightly interior to the Neptune orbit, at (25–27) AU. First, our analysis of a number of individual orbits has shown that the grains trapped in the resonance maintain the resonant value of a , while their orbital eccentricities e grow, so that the pericentric distances q decrease. The growth in e gradually slows down at some point, and so does the decrease in q . As a result, many resonant grains maintain $q \approx (25\text{--}27)$ AU over a long period of time. Second, a swarm of grains in Keplerian ellipses sharing the same q is known to reach a large (formally infinitely large) number density at the location of their pericenters, because the radial velocity of grains $\dot{r} = 0$ there (e.g., Eq. 2.13 in Krivov et al. 2005). Both effects together explain the sharp inner edges seen in Fig. 1. Jupiter, Saturn and, to lesser degree, Uranus contribute to the inner gap opening by gravitational scattering of dust drifting inward from the EKB.

3. MODEL WITH COLLISIONS

3.1. Method

1. As in Section 2, we start with distributing all the grains of size s into (x, y) -bins. This time, however, we will need to calculate the collisional rates and so need to know the

absolute number of different-sized particles in the system. Accordingly, we assume an initial size distribution $\propto s^{-q}$ and scale every particle by a certain normalizing factor ξ . Every grain (i.e., every record) is counted

$$\xi \left(\frac{s}{s_{\max}} \right)^{-q+1} \quad (1)$$

times, where s_{\max} is the largest grain size we considered. Although we will see later that the initial distribution of grains is overwritten by the collisional fragments, we assumed $q = 3.5$ which is the exponent for an idealized disk in a collisional equilibrium (Dohnanyi 1969). The +1 in the exponent is due to our using logarithmic size bins. This is done for each size listed in Table 2.

2. Treating the collisions, we assume them to occur between the colliders of the same size, so that the following procedure is done for every grain size separately. In our numerical integrations, we keep record of the velocity of every grain to calculate the mean relative velocity $\overline{v_{\text{rel}}}$ between *all* grains of size s in every spatial bin. Denoting by n the total number of records in an (x, y) bin obtained in step 1, the relative velocity is given by

$$\overline{v_{\text{rel}}}^2 = \frac{1}{n^2} \sum_{i,j=1}^n (\mathbf{v}_i - \mathbf{v}_j)^2 = \frac{2}{n} \sum_{i=1}^n \mathbf{v}_i^2 - \frac{2}{n^2} \left(\sum_{i=1}^n \mathbf{v}_i \right)^2, \quad (2)$$

where the indices i, j represent the single records of all particles¹. Typical relative velocities between two like-sized particles in the EKB region are (3–4) km s⁻¹ outside the clumps and $\lesssim 2$ km s⁻¹ inside them. Next, the mean collisional time in every (x, y) bin is calculated as

$$t_{\text{lif}}^{-1} = n\sigma\overline{v_{\text{rel}}}, \quad (3)$$

where $\sigma = 4\pi s^2$ is the collisional cross section for two colliders of radius s . Step 2 results in the knowledge of lifetime for every size in every (x, y) -bin, and we can start including collisions.

3. Once the lifetime is known, we repeated step 1 but this time counted every particle $\exp(-t/t_{\text{lif}})$ times, where t is the time elapsed after release from the parent body. This takes into account the loss due to collisions. Then we checked whether the grains of size s in question can be produced in collisions of larger grains s_{larger} and if so, the number of particles which are produced by larger grains was *added*. This was implemented as follows. When two particles of the same size collide with each other, the mass of the largest collisional fragment is (Krivov et al. 2006)

$$m_x \approx m_{\text{target}} \frac{Q_D^*(m_{\text{target}})}{\overline{v_{\text{rel}}}^2} \quad (4)$$

where m_{target} is the mass of one of the two colliders and Q_D^* is the critical specific energy which is needed to disrupt a particle² (e.g., Krivov et al. 2005):

$$Q_D^* = A(s/1 \text{ m})^{3b}. \quad (5)$$

¹Strictly speaking, the summation over i, j should run from 1 to n with $i \neq j$. Excluding $i = j$ would change the prefactor to $[n(n-1)]^{-1}$, but n is so large that the correction is negligible.

²A particle is considered disrupted when the largest fragment contains less than half of the mass of the original particle.

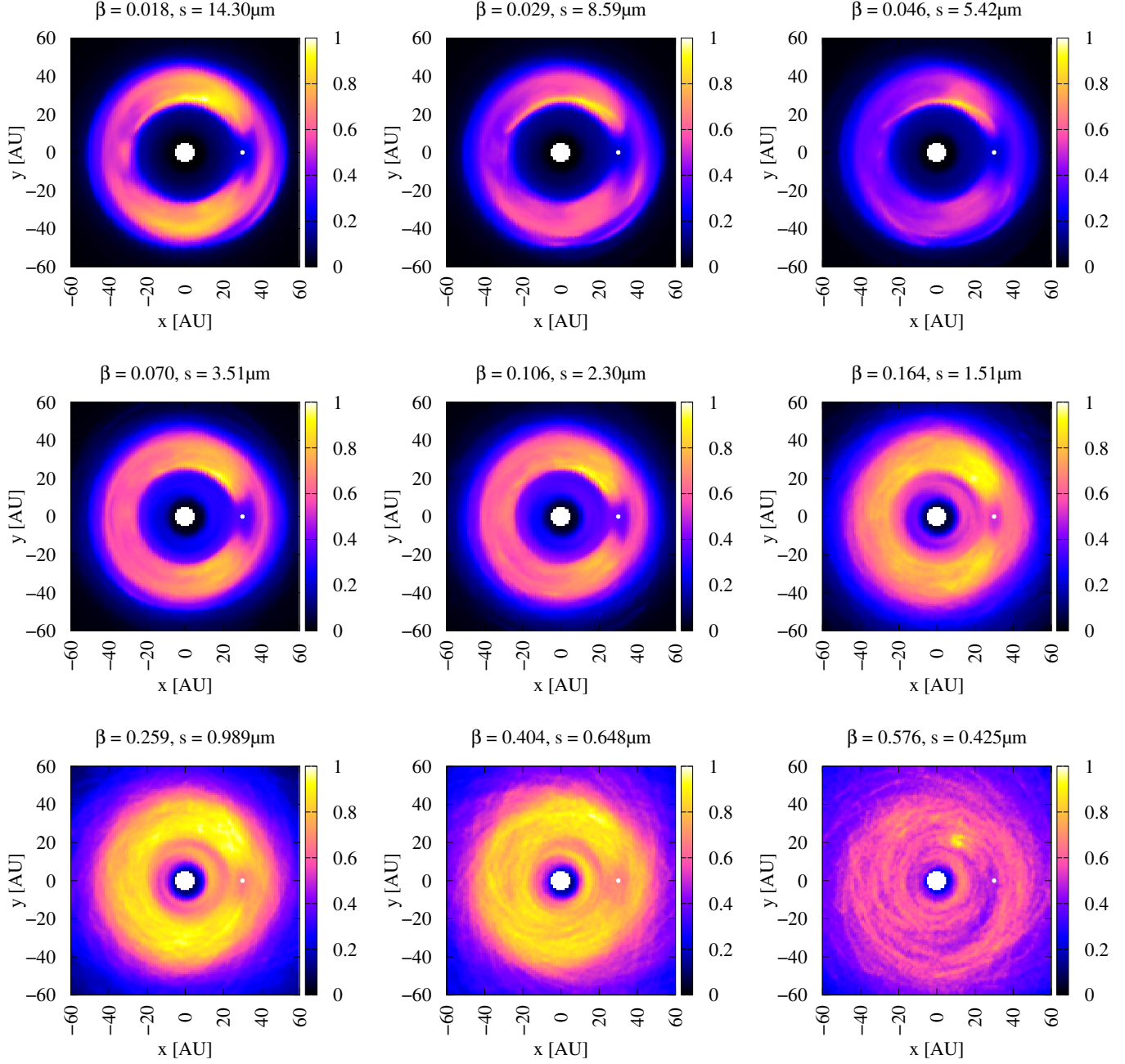


Fig. 1.— Number density in the ecliptic plane normalized to the densest bin (each size separately) for collisionless particles of different sizes. The small white dot is the location of Neptune.

As a nominal case, we took $A = 10^6 \text{ erg g}^{-1}$, $3b = -0.37$ (e.g., Benz & Asphaug 1999), but also tried other values to test how strongly the results can be affected by a poorly known strength of the dust material. Note that our largest dust grains are still far from being held together by gravity, so the gravity part of the equation is neglected and we only consider the strength regime. If the impact energy $E_{\text{imp}} = 0.25 m_{\text{target}} v_{\text{rel}}^2$ exceeds $2m_{\text{target}} Q_D^*$ (two objects of the same size have to be destroyed), the total mass of the target is fragmented, and we can write

$$m_{\text{target}} = \int \frac{4}{3} \pi \rho s^3 dN(s) = \int_0^{s_x} \frac{4}{3} \pi \rho s^3 N_0 \left(\frac{s}{s_x} \right)^{-p} ds$$

$$= \frac{4}{3} \pi \rho N_0 \frac{s_x^4}{4-p} \quad (6)$$

with s_x being the radius of the largest fragment (cf. Eq. 4). Here, $dN(s)$ is the fragment distribution function, N_0 its normalization constant, and the exponent p is assumed to be 3.5 (Fujiwara 1986). With this fragment distribution it is easy to calculate how many small grains of size s are produced:

$$n_{\text{prod}} = \left(\frac{s_{\text{larger}}}{s} \right)^3 \left[\left(\frac{s_+}{s_x} \right)^{4-p} - \left(\frac{s_-}{s_x} \right)^{4-p} \right]. \quad (7)$$

Since we use discrete sizes, s_- and s_+ are the minimum and maximum physical sizes represented by the size bin around s . We recall that n_{prod} is the number of grains s produced by *one* larger grain s_{larger} . Hence, we have to multiply it with the total number of larger grains n_{larger} in the same (x, y) -bin. Thus the number of the newly produced particles is

$$n_{\text{prod}} n_{\text{larger}} [1 - \exp(-t/t_{\text{life, larger}})], \quad (8)$$

where $[1 - \exp(-t/t_{\text{life, larger}})]$ is the fraction of larger grains already disrupted by collisions at time t . Finally, for one size in one (x, y) -bin we count every particle (i.e., every record)

$$\xi \left(\frac{s}{s_{\text{max}}} \right)^{-q} \underbrace{\exp(-t/t_{\text{life}})}_{\text{loss}} + \underbrace{n_{\text{prod}} n_{\text{larger}} [1 - \exp(-t/t_{\text{life, larger}})]}_{\text{gain}} \quad (9)$$

times. The gain term represents the particles which are produced by *all* particles larger than themselves.³ Note that this simple model tacitly assumes that small particles are produced by large ones locally. In particular, it does not include the radiation pressure effect on the newly produced particles immediately upon release. Nor does it include the drift of small particles inward from their birth location. This simplification is discussed in more detail in Sect. 5.

Steps 2 and 3 should be executed repeatedly, until the changes from iteration to iteration in each (x, y) -bin become smaller than the required accuracy. However, the convergence turned out to

be so fast that already the first iteration ensures the accuracy at a $< 10\%$ level. For this reason, in the calculations presented here we applied collisions only once.

Having calculated the number density, we can compute the particle flux on the SDC. It is given by

$$F = \int_{10^{-12} \text{ g}}^{10^{-9} \text{ g}} m \hat{n} v_{\text{imp}} d \ln m, \quad (10)$$

where m is the mass of the dust particle, \hat{n} is the number density per logarithmic mass m , and v_{imp} is their average velocity relative to the spacecraft. In practice, we replaced integration with summation over all mass bins $[m_-, m_+]$ that overlap fully or partly with the SDC sensitivity range $[10^{-12} \text{ g}, 10^{-9} \text{ g}]$. A logarithmic interpolation was applied between the bins and to the minimum (10^{-12} g) and maximum (10^{-9} g) detectable masses, since these do not coincide exactly with the bin boundaries m_- and m_+ . Furthermore, in Eq. (10) we replaced v_{imp} with the heliocentric velocity of New Horizons, v_{NH} . The latter was set to $v_{\text{NH}} = 15.5 \text{ km s}^{-1}$, the velocity New Horizons had shortly after the Uranus orbit crossing⁴, and assumed to be constant, although it decreases slightly with the increasing heliocentric distance. These simplifications introduce a velocity error not exceeding $(1-2) \text{ km s}^{-1}$ and thus a relative flux error of $\Delta F/F \lesssim 10\%$. This accuracy is sufficient, given the error bars of the SDC measurements (see Fig. 3). The trajectory of New Horizons was taken from the HORIZONS Web-Interface⁵.

3.2. Results

Figure 2 shows the snapshots produced after applying the collisions. It demonstrates clearly that resonant structures survive not only for larger, but also for smaller grains. This may seem in contradiction to Kuchner & Stark (2010) who showed that resonant structures will be washed out by destructive collisions, but they did not include production of grains. In fact it is the production of grains that is the most important part in our model. The initial distribution of small grains (bins #0–4) gets almost completely overwritten by small fragments supplied by collisions of larger grains.

One caveat is that, since we used nine sizes only, the largest grains (bins #5–8) do not have parent bodies in our calculation and hence are not replenished. On the other hand, sufficiently big impactors that could deplete the grains in the upper size bins are also absent. Thus the results presented for the largest grains ($\gtrsim 3 \mu\text{m}$) remain essentially collisionless. This explains that the panels in Figs. 1 and 2 for those sizes are nearly identical. However, the dust impact rates for New Horizons are unaffected, because they are dominated by smaller grains.

We now turn to the impact flux on the SDC. Like the number density, the flux depend on numerous model parameters describing the populations of EKBOs, collisional cascade physics, and dust properties. Although we can make an educated guess about all of them, many of these are not really known. Therefore, it is important to test the robustness of our model by varying diverse model parameters. To this end, we first define our nominal model as follows. As bulk density we use $\rho = 1.46 \text{ g cm}^{-3}$,

³Note that the “gain” term has to be divided by the number of records of like-sized particles in a certain (x, y) -bin from the collisionless analysis to avoid double counting.

⁴http://pluto.jhuapl.edu/mission/whereis_nh.php (Last accessed on 2011 Sep 2)

⁵<http://ssd.jpl.nasa.gov/horizons.cgi> (Last accessed on 2013 Sep 9)

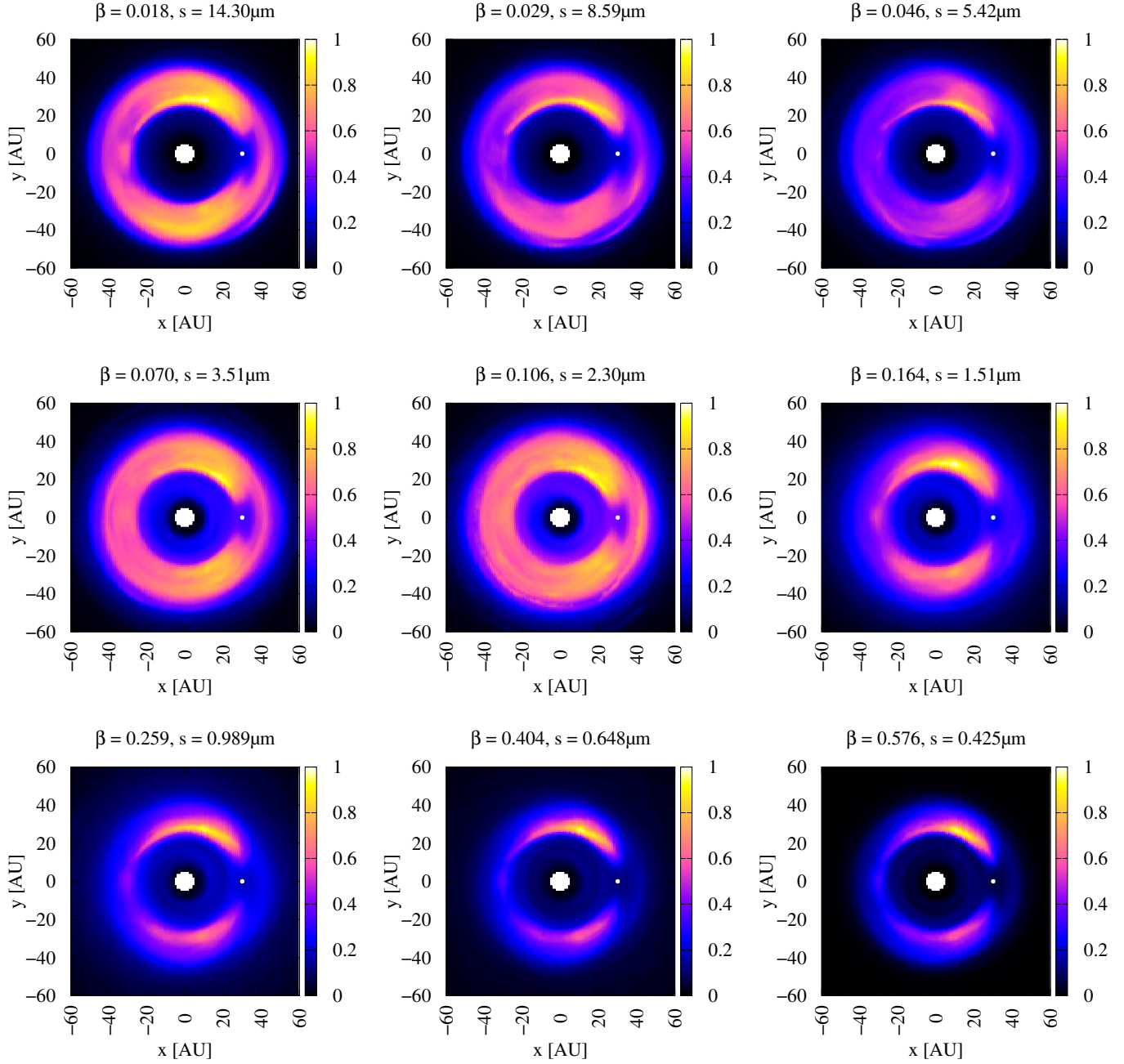


Fig. 2.— Same as Fig. 1 but after applying collisions.

the pre-factor of the critical specific disruption energy is set to $A = 10^6 \text{ erg g}^{-1}$, as exponent for the crushing law we adopted the standard value of $p = 3.5$. It is this model that we used in constructing Figs. 1-2. The fluxes for the nominal model are presented with the thick blue line in all panels of Fig. 3. Then we varied each of the values separately while leaving the others constant. The individual checks were done as follows:

1. *Bulk density and optical properties of dust.* As compositions we used the three different material mixtures introduced in Table 2. The corresponding fluxes are shown in the top left panel of Fig. 3. There is a slight trend towards a higher particle flux in the clumps for grains with a lower ice content (or with a higher bulk density). Yet the difference is much smaller than the data point error bars, and hence the bulk density cannot be constrained further.
2. *Mechanical strength of dust.* We have checked the sensitivity of our results to the critical specific energy Q_D^* which is not reliably known either. We tried to replace $A = 10^6 \text{ erg g}^{-1}$ with $A = 5 \times 10^6 \text{ erg g}^{-1}$ and $A = 2 \times 10^5 \text{ erg g}^{-1}$. The results are shown in the top right panel of Fig. 3. As expected, increasing the material strength weakens collisional erosion, requiring less material in the outer region to explain the observed flux in the Uranus-Saturn region. However, the difference between the curves is still minor and there is little hope that the New Horizons data could help constraining the material strength — unless A deviates from the nominal value by more than an order of magnitude.
3. *Collisional physics.* We investigated the influence of the exponent of the crushing law that determines the size distribution of fragments of any destructive collision. While assuming $p = 3.5$ in the nominal case, we also tried $p = 2.5$ and $p = 3.8$. The bottom left panel shows the result of this variation. Here, too, the differences are too small to be measurable by the SDC.
4. *Parent body populations.* One more potentially important uncertainty in our model is related to the dust parent bodies. While the true amount and orbital element distributions of classical and resonant populations are thought to be known reasonably well, those of the scattered disk objects are not (Vitense et al. 2010). Reliable estimates for SDOs are not possible because of their high eccentricities and large semimajor axes. To check the potential effect, we used the “true” SDO population derived by Vitense et al. (2010) in the nominal model, but also tested the extreme cases of no SDOs and twice as many SDOs as in the nominal model. The results are presented in the bottom right panel. With twice as many SDOs there is a marginal decrease of dust flux in the clumps. Albeit too small to be detectable, the very effect is interesting. When dust particles are released from SDOs their semimajor axes and eccentricities are higher than if they are released from classical objects. Then, the PR drag decreases both a and e . Nevertheless, when they finally reach the location of the 3 : 2 resonance, the eccentricities are still higher than those of the particles released by classical objects. As a result, the probability of being captured into the mean motion resonance is lower (Mustill & Wyatt

2011), decreasing the dust density in the clumps. Moreover, when these highly eccentric particles enter the region between Saturn and Uranus, they have higher mean relative velocity and experience more disruptive collisions, which enhances the dust concentration there. However, since we fit the modeled fluxes to the SDC measurements at those locations, they are “nailed” to the data points, which further decreases the height of the flux curve in the clumps.

Beside the parameter variation, one more test was needed for the following reason. The results presented above were obtained by counting the particles with all z -coordinates, implicitly assuming that the dust disk is uniform vertically. However, this is not true, and New Horizons has a non-zero inclination of $i_{\text{NH}} = 2.4^\circ$. To check how this could affect the rates, we have done a separate calculation where we only considered particles with $0 < z < r \sin i_{\text{NH}}$. After fitting the resulting curve to the available data, we found it to be nearly indistinguishable from the nominal curve.

From all these tests, we argue that New Horizons should be able to detect the increased impact fluxes when entering the clumps. The conclusion holds if the poorly known model parameters are varied within physically plausible ranges.

Figure 3 presents the particle flux averaged over the heliocentric longitude. A pole-on (and therefore spatially resolved) view is given in Fig. 4. It reveals that the clumps are not entirely symmetric. The dust flux in the Neptune-trailing clump (which will be flown through by New Horizons) should be slightly lower than in the leading one.

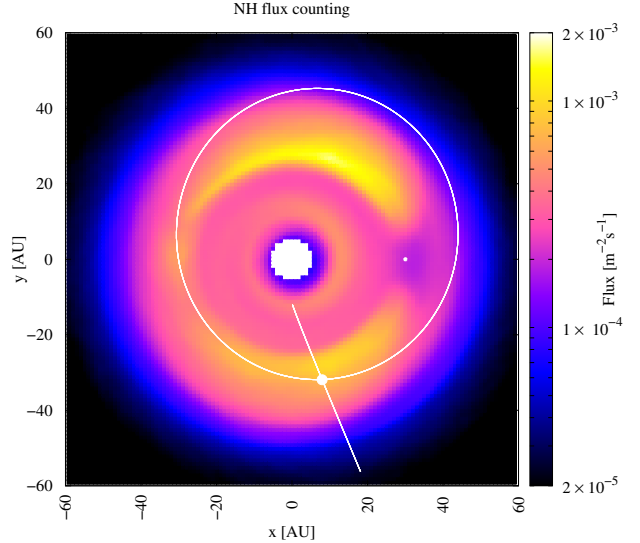


Fig. 4.— Pole-on view of the modeled particle flux in our nominal model. The white ellipse represents the orbit of Pluto, the white line toward bottom left is the trajectory of New Horizons, the small white dot is the location of Neptune, and the big white dot the intersection between New Horizons and Pluto.

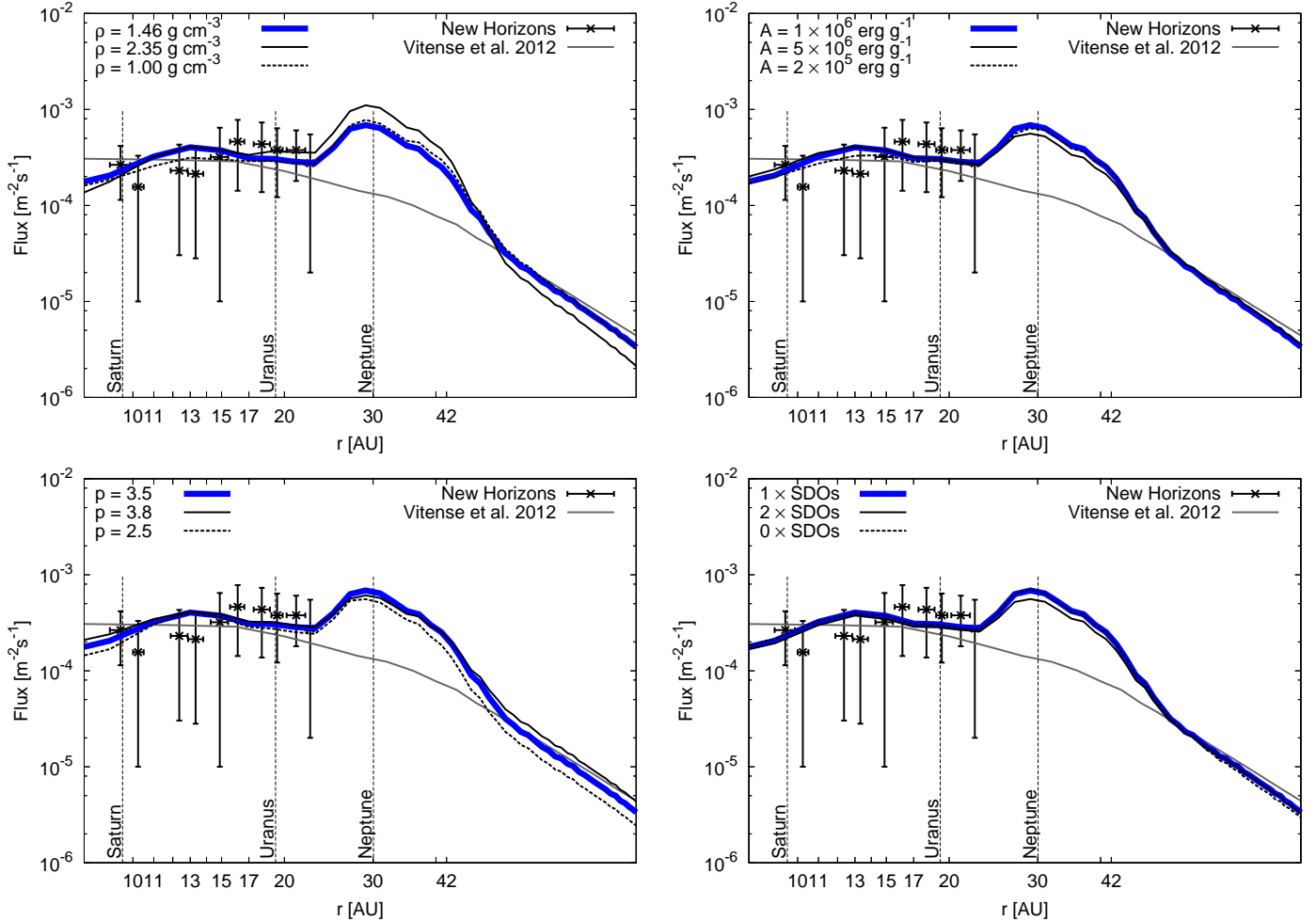


Fig. 3.— Modeled particle flux (lines) fitted to the in-situ measurements of New Horizons (symbols with $1\text{-}\sigma$ error bars). The thick blue line is the same in all four panels and represents our nominal model (ice-silicate mixture with $\rho = 1.46 \text{ g cm}^{-3}$, material strength with $A = 10^6 \text{ erg g}^{-1}$ in Eq. 5, the crushing law exponent $p = 3.5$, SDO populations from Vitense et al. 2010). Individual panels show the dependence of the flux on the assumed material composition (top left), material strength (top right), the crushing law exponent (bottom left), and the assumed number of SDOs (bottom right). Grey line is a rotationally symmetric model of Vitense et al. (2012) for comparison. The data are taken from Poppe et al. (2010), Han et al. (2011), and Szalay et al. (2013).

4. CONCLUSIONS

In this paper we developed a model to reproduce and predict dust impact rates onto the dust detector of New Horizons. To this end, we used the debiased EKBO populations from Vitense et al. (2010) and launched 27000 dust grains of nine sizes. The particle sizes were chosen in such a way as to cover the entire mass sensitivity range of the dust detector aboard New Horizons. We then integrated their orbits by including the gravity of the four giant planets, stellar wind and the Poynting-Robertson effect, and recorded the position and velocities every orbit of Neptune. The resulting 2×10^9 records were used to draw a collisionless dust density map. We then complemented this collisionless model with a post-processing algorithm to roughly simulate a collisional cascade.

In the collisionless approximation, our model fully reproduces the results obtained previously with similar methods. The most salient feature of all collisionless models, pioneered by the Liou & Zook (1999) study, is a pair of resonant clumps ahead and behind the Neptune location. These clumps are dominated

by grains that are large enough to be efficiently captured in resonances with Neptune.

Including collisions has a potential of changing the number density map for small (submicrometer-sized) grains dramatically. Since it is these grains that are predominantly detected by the New Horizons dust detector, the issue is important. Kuchner & Stark (2010) made the first attempt to include collisions in the models of azimuthal structure in the EKB region and showed that the collisional elimination of grains should essentially wash out the clumps. However, they only considered collisional loss of grains. Our model refines theirs by adding the collisional replenishment of small grains. This tends to increase the amount of dust in the clumps almost back to the level predicted by the collisionless models.

We have calculated the dust impact fluxes onto the New Horizons dust detector to find that it should be able to detect an increase of particle flux when it enters the region of the clump ahead the position of Neptune. The dust flux should increase by a factor of two or three. By varying the assumed material

composition, mechanical strength of dust and the exponent of the crushing law, we checked that this result is rather robust, making our predictions quite certain. At the same time, this implies that New Horizons will probably not be able to provide additional constraints on the dust properties. The same applies to uncertainties stemming from a poorly known distribution of the dust parent bodies, especially of the scattered population of the Kuiper belt objects. Including or excluding this population from the simulations does not affect the predicted impact rates considerably.

5. DISCUSSION

Although we did check that our predictions should not strongly depend on the unknown properties of the dust grains and detailed distributions of dust-producing Kuiper belt objects, the model itself necessarily involves a number of simplifications, assumptions, and omissions that may affect the results. Apart from standard assumptions, such as that of spherical particles or using the Mie theory for radiation pressure calculations, caveats exist in our simulations of the collisional cascade. While we improved previous EKB dust models, complementing collisional depletion by collisional production, we assumed, for instance, equal-size impactors. Collisions between different-sized impactors would lead to somewhat higher collisional velocities and rates and thus increase the total number of collisionally produced small particles, resulting in a higher dust flux. Nevertheless, since we are fitting our model to the data of New Horizons, the “missing” flux will automatically be compensated by a larger ξ in Eq. 1.

Even more importantly, we did not include radiation pressure on newly produced particles. After a disruptive collision between large grains, small particles gain orbital energy from radiation pressure which sends them onto a different, usually eccentric and wide, orbit. This may spread the clumps, decreasing the dust density enhancement compared to what our model predicts, closer to what previous models without collisional production suggest. Nevertheless, we do not think that the structures would be completely washed away. First, after spreading, the particles will drift back inward and many will be re-captured into resonances. Even for small particles (sizes #2 and #3) a slight enhancement can be seen at the location of resonances. Second, the highest collision rates are in the clumps, hence there is an enhanced production and thus a higher number density of fine grains there (Wyatt 2006). Third, the pericenters of collisionally produced dust particles will always lie at their birth point and thus — in contrast to their apocenters — are not subject to radiation pressure spreading (see discussion at the end of Sect. 2.2). Altogether, we believe the “true” distribution of dust is somewhere between previous models and ours, perhaps closer to the latter. This is to say that New Horizons might measure a more moderate enhancement of the impact rate when traversing the clump than our model predicts.

There are also other factors that might decrease the enhancement. One of them is the “sporadic” dust background stemming from sources other than EKBOs, e.g. Trojans, Centaurs, or comets of Schwassmann-Wachmann type (Landgraf et al. 2002). Some contribution can also be made by interstellar grains, especially given that New Horizons is facing the upstream direction of the interstellar dust flow. However, Altobelli et al. (2007) showed that the interstellar grains of size $s \approx 0.4 \mu\text{m}$ contribute

to the overall dust flux by $F = 2 \times 10^{-5} \text{ m}^{-2} \text{ s}^{-1}$ which is an order of magnitude below the measurements of the SDC and therefore can be neglected. The possibilities to make the clumps *more pronounced* than predicted here are more limited. Should the enhancement seen by the SDC be stronger than expected, this could be attributed, for instance, to a lower critical disruption energy or to a higher bulk density of dust particles.

We would like to thank Martin Reidemeister for a helpful discussion of several numerical aspects of this work. Useful comments by the anonymous reviewer are appreciated. This research was partly supported by the *Deutsche Forschungsgemeinschaft* (DFG), projects number Lo 1715/1-1 and Kr 2164/10-1.

REFERENCES

- Altobelli, N., Dikarev, V., Kempf, S., et al. 2007, *Journal of Geophysical Research (Space Physics)*, 112, 7105
- Artymowicz, P., & Clampin, M. 1997, *ApJ*, 490, 863
- Benz, W., & Asphaug, E. 1999, *Icarus*, 142, 5
- Bohren, C. F., & Huffman, D. R. 1983, *Absorption and Scattering of Light by Small Particles* (Wiley and Sons: New York – Chichester – Brisbane – Toronto – Singapore)
- Burns, J. A., Lamy, P. L., & Soter, S. 1979, *Icarus*, 40, 1
- Debes, J. H., Weinberger, A. J., & Kuchner, M. J. 2009, *ApJ*, 702, 318
- Dermott, S. F., Jayaraman, S., Xu, Y. L., Gustafson, B. Å. S., & Liou, J. C. 1994, *Nature*, 369, 719
- Dohnanyi, J. S. 1969, *J. Geophys. Res.*, 74, 2531
- Fujiwara, A. 1986, *Mem. Soc. Astron. Italiana*, 57, 47
- Greaves, J. S., Holland, W. S., Wyatt, M. C., et al. 2005, *ApJ*, 619, L187
- Grigorieva, A., Artymowicz, P., & Thébault, P. 2007, *A&A*, 461, 537
- Gustafson, B. A. S. 1994, *Annual Review of Earth and Planetary Sciences*, 22, 553
- Han, D., Poppe, A. R., Piquette, M., Grün, E., & Horányi, M. 2011, *Geophys. Res. Lett.*, 38, 24102
- Horányi, M., Hoxie, V., James, D., et al. 2008, *Space Science Reviews*, 140, 387
- Kalas, P., Graham, J. R., Fitzgerald, M. P., & Clampin, M. 2013, *ApJ*, 775, 56
- Kalas, P., Graham, J. R., Chiang, E., et al. 2008, *Science*, 322, 1345
- Krivov, A. V., Löhne, T., & Sremčević, M. 2006, *A&A*, 455, 509
- Krivov, A. V., Sremčević, M., & Spahn, F. 2005, *Icarus*, 174, 105
- Kuchner, M. J., & Stark, C. C. 2010, *AJ*, 140, 1007

- Lagrange, A.-M., Gratadour, D., Chauvin, G., et al. 2009, *A&A*, 493, L21
- Lagrange, A.-M., Bonnefoy, M., Chauvin, G., et al. 2010, *Science*, 329, 57
- Lagrange, A.-M., Boccaletti, A., Milli, J., et al. 2012, *A&A*, 542, A40
- Landgraf, M., Liou, J.-C., Zook, H. A., & Grün, E. 2002, *AJ*, 123, 2857
- Laor, A., & Draine, B. T. 1993, *ApJ*, 402, 441
- Liou, J.-C., & Zook, H. A. 1999, *AJ*, 118, 580
- Moro-Martín, A., & Malhotra, R. 2002, *Astron. J.*, 124, 2305
- . 2003, *AJ*, 125, 2255
- Mustill, A. J., & Wyatt, M. C. 2011, *MNRAS*, 413, 554
- Poppe, A., James, D., Jacobsmeyer, B., & Horányi, M. 2010, *Geophys. Res. Lett.*, 37, 11101
- Press, W. H., Teukolsky, S. A., Vetterling, W. T., & Flannery, B. P. 1992, *Numerical recipes in C. The art of scientific computing* (Cambridge: University Press, 1992, 2nd ed.)
- Rameau, J., Chauvin, G., Lagrange, A.-M., et al. 2013, *ApJ*, 772, L15
- Su, K. Y. L., Rieke, G. H., Stapelfeldt, K. R., et al. 2009, *ApJ*, 705, 314
- Szalay, J. R., Piquette, M., & Horányi, M. 2013, *Earth, Planets and Space*, 65, 1145
- Vitense, C., Krivov, A. V., Kobayashi, H., & Löhne, T. 2012, *A&A*, 540, A30
- Vitense, C., Krivov, A. V., & Löhne, T. 2010, *A&A*, 520, A32
- Warren, S. G. 1984, *App. Optics*, 23, 1206
- Wyatt, M. C. 2003, *ApJ*, 598, 1321
- . 2005, *A&A*, 440, 937
- . 2006, *ApJ*, 639, 1153